Japanese Journal of Applied Physics
Vol. 44, No. 1B, 2005, pp. 662–668

Growth and Electrochemical Properties of Single-Crystalline V_2O_5 Nanorod Arrays

Katsunori TAKAHASHI[1,2], Steven J. LIMMER[1], Ying WANG[1] and Guozhong CAO[1,*]

[1]*Department of Materials Science and Engineering, University of Washington, 302 Roberts Hall, Box 352120, Seattle WA 98195 U.S.A.*
[2]*Steel Research Laboratory, JFE Steel Corporation, 1 Kawasaki-cho, Chuo-ku, Chiba 260-0835, Japan*

(Received July 9, 2004; accepted October 29, 2004; published January 24, 2005)

Growth and electrochemical properties of single-crystalline vanadium pentoxide (V_2O_5) nanorod arrays were investigated. Vanadium pentoxide nanorod arrays were grown by electrochemical deposition, surface condensation induced by a pH change and sol electrophoretic deposition. Uniformly sized vanadium oxide nanorods with a length of about 10 μm and diameters of 100 or 200 nm were grown over a large area with near-unidirectional alignment. Transmission electron microscopy (TEM) micrographs and electron diffraction patterns of V_2O_5 nanorods clearly show the single-crystalline nature of nanorods fabricated via all three growth routes with a growth direction of [010]. The growth mechanisms of single-crystal V_2O_5 nanorods have been discussed. Electrochemical analysis revealed that nanorod array electrodes possess significantly improved storage capacity and charge/discharge rate with approximately 5 times higher applicable current density than those of sol-gel derived films. Furthermore, for a given current density, the nanorod array electrode can intercalate up to 3.5 times higher concentration of Li^+ intercalation. The relationships between electrochemical property, nano- and microstructure, and growth mechanisms have been discussed. [DOI: 10.1143/JJAP.44.662]

KEYWORDS: nanorod arrays, single-crystal growth, electrochemical deposition, electrophoretic deposition, lithium intercalation

1. Introduction

A great deal of attention has been focused on the synthesis and applications of nanostructured materials, and many synthesis and processing techniques have been developed.[1,2] One of the most dynamic research areas is the synthesis of one-dimensional nanostructures, such as nanowires, nanorods, and hollow tubes.[3–7] Template-based synthesis is one of the most common fabrication methods of nanorod arrays, particularly for mass production and alignment, since this method offers the ability to fabricate unidirectionally aligned and uniformly sized nanorod arrays of a variety of materials. Nanorods of numerous materials including metals, semiconductors, polymers, oxides, and composites have been formed by this technique.[8–10] Various methods have been developed to fill the pores of template membranes for the formation of nanorod or nanowires.[11,12] For example, electrochemical deposition, also commonly referred to as electrodeposition, is generally used for the growth of electrically conductive materials, such as metals, semiconductors, and conductive polymers.[1] In electrophoretic deposition, the electric field induces oriented migration and stacking of charged nanoclusters or nanoparticles on the growth surface, and no electrochemical reactions at the growth surface are required.[13] Therefore, electrophoretic deposition can be used for the growth of dielectric materials, and various dielectric oxide nanorods have been synthesized using a combination of electrophoretic deposition and sol-gel processing.[14,15]

Vanadium pentoxide has attracted much attention, for example as an electrode material for electrochemical pseudocapacitor applications due to its intercalation ability, among many other applications such as electrochromic coatings[16] and actuators.[17] V_2O_5 has a layered structure and has the ability to intercalate ions between adjacent layers.[18] This intercalation process is accompanied by a change of dimension, due to the expansion or contraction of the distance between adjacent layers, and a change of color, due to the change of valence states of vanadium ions. When V_2O_5 intercalates Li^+, electrical energy is stored in the form of chemical potential. Energy is released from V_2O_5 in the form of electricity, when the intercalated Li^+ diffuses out. For electrochemical pseudocapacitor applications, charge/discharge rate, energy storage capacity, and cyclic fatigue resistance are the most important parameters. A large surface area and easy transport are required to achieve a high charge/discharge rate.[19,20] Since only a thin surface layer is active in the intercalation process,[21] a large surface area is also desirable to achieve large storage capacity. In addition, the ability of free expansion and contraction of vanadium pentoxide is needed to permit efficient intercalation and discharge with good fatigue resistance. It is clear that nanorod arrays of single-crystal vanadium oxide are a promising structure for realizing high capacity, fast charge and discharge kinetics, and improved fatigue resistance. Recently, we have demonstrated that single-crystal V_2O_5 nanorod arrays have approximately 5 times higher applicable current density than sol-gel-derived film, and in a given current density, a nanorod array electrode can intercalate up to 5 times higher concentration of lithium ions.[22] In this paper, we report the study on the growth of single-crystal vanadium pentoxide (V_2O_5) nanorod arrays from three aqueous solutions or sol by electrochemical and electrophoretic deposition, and their electrochemical properties. The possible growth mechanisms of single-crystal vanadium oxide nanorod arrays and the relationship between the electrochemical properties and nanostructures are discussed.

2. Experimental

2.1 Preparation of solutions and sol

The chemicals used in making solutions and sol were V_2O_5 (Alfa Aesar), 30% H_2O_2 (J.T. Baker), $VOSO_4 \cdot nH_2O$ (Alfa Aesar), HCl (37.5%, Fisher) and H_2SO_4 (96.5%, Fisher). Two ionic solutions and one sol were prepared from the above chemicals using the following procedures.

A VO^{++} solution was prepared by dissolving $VOSO_4 \cdot nH_2O$ into deionized water together with H_2SO_4 in

*E-mail address: gzcao@u.washington.edu

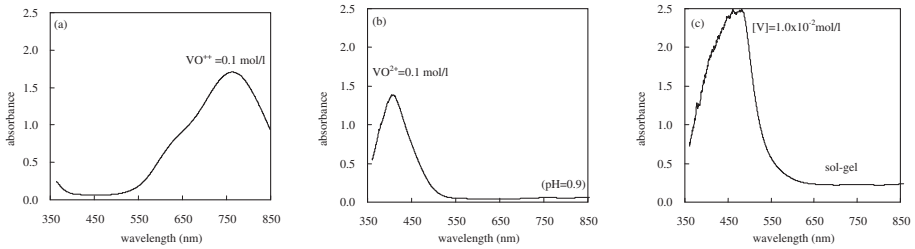

Fig. 1. Optical absorption spectra of vanadium solution/sol: (a) VO^{++} solution, (b) VO_2^+ solution with varied pH, (c) sol C.

a molar concentration of 0.1 mol/l as $n = 5.0$, with a pH of 1.5. Such a solution has a blue color with a broad absorption peak centered around 750 nm and a weak shoulder at ~630 nm as shown in Fig. 1(a). Both peaks correspond to the VO^{++} cluster[23] (the valence state of vanadium ion is 4+). This solution is stable within a wide range of pH and vanadium ionic cluster concentrations.

A 0.1 mol/l VO_2^+ solution was prepared by dissolving V_2O_5 gel into H_2SO_4 aqueous solution. V_2O_5 gel was synthesized by the method reported by Fontenot *et al.*[24] V_2O_5 powder was dissolved in H_2O_2 solution with a V_2O_5 concentration of 0.15 mol/l. HCl was added to stabilize VO_2^+ and $VO(O_2)(H_2O)^{3+}$ ionic clusters. The resulting solution had a H_2O_2/V_2O_5 ratio of 8:1 and HCl/H_2O_2 ratio of 1/10. After stirring for 90 min at R.T., excess H_2O_2 was decomposed by sonication, and a yellow-brown gel was obtained. The gel was then dissolved in a H_2SO_4 aqueous solution, at a concentration of 0.1 mol/l vanadium ions. The resultant solution has a pH of ~1.0 and the primary vanadium ionic clusters are VO_2^+, which have a yellow-green color with a strong absorption band at around 400 nm and a weak peak at ~750 nm (as shown in Fig. 1(b)). Such an absorption spectrum is characteristic of VO_2^+ ionic clusters (here vanadium ion has a valence state of 5+).[23]

V_2O_5 sol was made by redispersing the above yellow-brown gel in DI water. The sol has a brownish color and contains 0.01 mol/l vanadium ions with a pH of 2.7. The primary vanadium species in the colloidal dispersion are mainly hydrated vanadium oxide nanoparticles with one observable absorption peak at 450 nm (Fig. 1(c)). However, a small amount of ion clusters may also be present, as suggested in literature.[24]

2.2 *Growth of nanorod arrays*

Vanadium pentoxide nanorod arrays have been grown inside polycarbonate templates with the assistance of an electric field. The templates used for this study were radiation track-etched hydrophilic PC membrane (Millipore, Bedford, MA) with pore diameters of 200 nm and thickness of 10 μm. To ensure a good electrical contact, the back of the membrane template was first sputter-coated with Au-Pd alloy before being attached to the working electrode. An aluminum sheet of 9 mm diameter was used as the working electrode placed beneath the template, and a Pt mesh was used as a counter electrode. The distance between the two electrodes was kept at 25 mm. A detailed description of the deposition setup can be found in our previous publications.[14,15] The applied electric voltage ranges from 0.3 to 2.5 V, and the deposition lasted up to 2 h. Upon the completion of deposition, the samples were dried at 110°C for 12 h in air, and then fired at 485°C in air for 1 h to remove the polycarbonate membranes through pyrolysis and oxidation. For comparison, sol-gel-derived vanadium pentoxide film was also prepared by dip coating, followed by firing at 485°C for 1 h in air. Such a prepared sol-gel film is uniform and crack-free, with has a thickness of ~1 μm.

2.3 *Characterization and electrochemical property measurement*

Optical absorption spectra of solutions and sols with various concentrations were carried out in the range of 400 nm to 900 nm using a fiber optic spectrometer (Ocean Optics PC2000). Scanning electron microscopy (SEM, JEOL JSM-5200) was used to characterize the morphology of nanorod arrays. Transmission electron microscope (TEM) images and electron diffraction patterns were recorded using Phillips EM420 and JEOL 2010 microscopes at accelerating voltages of 120 kV (Phillips) and 200 kV (JEOL). The crystal structure and crystal orientation of nanorods, gel powders and films before and after firing were studied by X-ray diffractometry (XRD, Philips PW1830).

Electrochemical properties of nanorod arrays and sol-gel films were investigated using a three-electrode cell. The vanadium pentoxide nanorod array electrode was made by attaching a PC membrane with grown V_2O_5 nanorods onto an ITO substrate with silver paste, dried first at 110°C for 8 h, and then heated at 485°C for 1 h in air to pyrolyze the PC membrane. For the sol-gel film, vanadium pentoxide sol was directly coated onto the ITO substrate and fired at 485°C in air for 1 h. The apparent surface area of the electrode is 6.4×10^{-5} m^2. A 1 M-$LiClO_4$ solution in propylene carbonate is used as the electrolyte, and a platinum mesh is used as the counter electrode with $Ag/AgNO_3$ as a reference electrode. A cyclic voltammetry measurement was carried out using potentiostat/galvanostat (EG&G Princeton Applied Research, model 273).

3. Results and Discussion

Figure 2 shows SEM images of V_2O_5 nanorod arrays grown in the PC membranes with pore diameters of 200 nm, and fired at 485°C for 1 h in air from the three different solutions and sol by either electrochemical or electrophoretic deposition. The images show that these nanorods are arranged almost parallel to one another over a broad area; the distortion is ascribed to the deformation of the PC membrane during pyrolysis. There is negligible shrinkage along the long axis, but the morphology and diameter of nanorods grown from different solutions or sol are different.

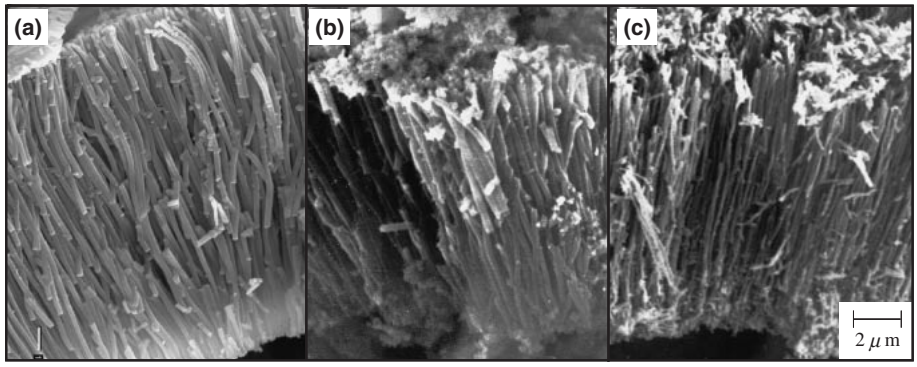

Fig. 2. SEM images of V_2O_5 nanorods grown in a PC membrane with 200 nm diameter pores; (a) from $VOSO_4$ solution, (b) from $[VO_2^+]$ solution with pH change, (c) from sol-gel route grown on a positive electrode. (a) on positive: reaction generates an electron: $2VO^{++} + 3H_2O \rightarrow V_2O_5 + 6H^+ + 2e^-$ (b) on negative: precipitate reaction according to local pH rising: $2VO_2^+ + H_2O \rightarrow V_2O_5 + 2H^+$ (c) on positive: electrophoretic deposition (zeta potential = 0 at pH = 1.825)

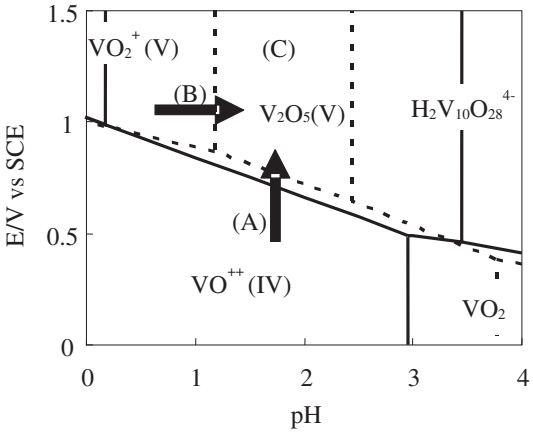

Fig. 3. Calculated potential-pH predominant diagram for vanadium oxide species in aqueous solution based on kinetic equilibrium. Solid line shows [V] = 0.1 mol/l and dash shows [V] = 0.01 mol/l.

Nanorods grown from solutions A and B have a uniform diameter throughout their entire length with a smooth surface, but in the case of solution C, nanorods have a narrower diameter and a slightly rough surface. XRD spectra indicate that all nanorod arrays have the same crystal structure vanadium pentoxide after firing at 485°C, regardless of the growth method and the initial solution.

Figure 3 illustrates the three different growth routes used for the formation of vanadium oxide nanorod arrays. More specifically, nanorod arrays in Fig. 2(a) were grown from a VO^{++} ionic cluster solution by electrochemical deposition (route A). Those in Fig. 2(b) correspond to route B, in which deposition of V_2O_5 was accomplished through the change of valence state of vanadium ions induced by the increase of pH near the growth surface as a result of water electrolysis in VO_2^+ ionic cluster solution, whereas nanorod arrays in Fig. 2(c) were formed by sol electrophoretic deposition from V_2O_5 sol. Table I summarizes the electrode conditions and shrinkage percentages of vanadium pentoxide nanorod arrays grown via these three different routes. It is noted that under similar growth conditions, nanorods grown by electrochemical deposition exhibited a negligible shrinkage, whereas those grown by changing the pH showed a appreciable lateral shrinkage of 15%. Moreover, nanorods

Table I. Growth conditions and amount of shrinkage of vanadium pentoxide nanorod arrays fabricated via the three different routes.

	Route	Vanadium species	Growth electrode	Shrinkage after firing
A	valence change	VO^{++} ion	(+)	0%
B	pH change	VO_2^+ ion	(−)	15%
C	sol-gel	colloid	(+)	50%

grown by sol electrophoretic deposition underwent a substantial lateral shrinkage of 50%. Such large differences in lateral shrinkage of the three type of nanorods upon firing can be explained by their distinctively different growth mechanisms.

The growth of nanorods from VO^{++} solution (route A) is by a typical electrochemical deposition. At the interface between the electrode (and subsequent growth surface) and electrolyte solution, the ionic cluster, VO^{++}, is oxidized and solid V_2O_5 is deposited through the following reaction.

$$2VO^{++} + 3H_2O \rightarrow V_2O_5 + 6H^+ + 2e^- \quad (1)$$

A reduction reaction takes place at the counter electrode:

$$2H^+ + 2e^- \rightarrow H_2(g) \quad (2)$$

It is obvious that pH and the concentration of VO^{++} clusters in the vicinity of the growth surface shift away from that in the bulk solution; both pH and VO^{++} concentration decrease. However, the change of pH and VO^{2+} cluster concentration does not lead to the formation of a new chemical species, as evidenced in Fig. 3. High voltage is likely to induce a fast growth rate until diffusion becomes the rate limiting step.

Growth from VO_2^+ solution (route B) has a different mechanism. Electrochemical reactions also take place at the interface between the deposition electrode (or the growth surface) and the electrolyte solution:

$$2H_2O + 2e^- \rightarrow H_2 + 2OH^- \quad (3)$$

$$2VO_2^+ + 2OH^- \rightarrow V_2O_5 + H_2O \quad (4)$$

Reaction 3, or the electrolysis of water, plays a very important role here. First, as the reaction proceeds, more hydroxyl groups are produced, resulting in an increased pH

value near the deposition surface or a change of local pH values. Such an increase of pH near the growth surface initiates and promotes the precipitation of V_2O_5, or reaction 4. The sequential reactions can be easily understood from Fig. 3. The initial pH of solution B is approximately 1.0, in which VO_2^+ is metastable. However, when pH increases to $\sim$1.8, V_2O_5 forms. The hydrolysis of water has another effect on the deposition of solid V_2O_5. Reaction 3 produces hydrogen on the growth surface. Such molecules may poison the growth surface before dissolving into the electrolyte or forming a gas bubble, which may cause the formation of porous nanorods, which shrink when fired at 485°C.

Growth from sol (route C) is a by typical electrophoretic deposition. In this method, an externally applied electric field induces oriented migration of vanadium oxide nanoclusters, which have a negatively charged surface at a pH of 2.7, since the isoelectric point of vanadia is around 1.8. When these charged nanoclusters are packed or deposited on the electrode or growth surface, the electrostatic double layer surrounding each nanocluster collapses under the externally applied electric field. As is common in a typical electrophoretic deposition process, no electrochemical reaction is required. How well the nanoclusters are packed on the growth surface depends on many factors such as the concentration of the nanoclusters in the sol, the strength of the applied electric field, the reaction rate of surface condensation between two nanoclusters, and the morphology of the nanoclusters. The maximum achievable packing density is $\sim$74% assuming nanoclusters are monosized and spherical; nanorods grown by sol electrophoretic deposition (route C) are always porous and thus are expected to undergo large shrinkage upon firing.

Figure 4 shows typical TEM micrographs and selected-area electron diffraction patterns of V_2O_5 nanorods grown by electrochemical deposition (route A) and sol electrophoretic deposition (route C). No appreciable difference was observed among nanorods grown by three different methods. These diffraction patterns clearly proved the single-crystalline or, at least, well oriented nature of the nanorods. All of the diffraction patterns can be indexed as orthorhombic V_2O_5 on a [001] zone axis. When the image of the nanorod is overlaid on the diffraction pattern, one observes that the long axis of the nanorod points towards the (020) spot. Thus, if growth occurs along the length of the nanorod, this information suggests a [010] growth direction for the nanorods. Figure 4 also shows high-resolution TEM micrographs of a single V_2O_5 nanorod, in which lattice fringes are clearly visible. The spacing of the fringes was measured to be 0.207 nm for nanorods made from solutions, and 0.208 nm for those made from the sol. These values are similar for different synthesis routes and correspond well with the spacing of (202) planes at 0.204 nm. These fringes make an angle of 88.9° with the long axis of the nanorod, which is consistent with a growth direction of [010]. Similar measurements made on high-resolution images of other nanorods also yield results consistent with a [010] growth direction. However, these measurements do not definitely prove that [010] is the growth direction.

Nanorods with the same orientation are grown from both solutions and the sol, but the formation mechanism of the single crystal is different, as schematically illustrated in Fig. 5. The formation of single-crystal nanorods from solutions, by both electrochemical deposition and pH-change induced surface condensation, is attributed to evolution selection growth, which is briefly summarized below. The initial heterogeneous nucleation or deposition on the substrate surface results in the formation of nuclei with random orientations. The subsequent growth of various facets of a nucleus is dependent on the surface energy, and varies significantly from one facet to another.[25] For one-dimensional growth, such as film growth, only the highest growth rate in the direction perpendicular to the growth surface will continue to grow. The nuclei growing perpendicular to the growth surface, along which the growth rate is the fastest, will grow larger, while nuclei with slower growth rates will eventually cease to grow. Such a growth mechanism results in the formation of columnar structured films with all the grains having the same crystal orientation (known as textured films).[26,27] In the case of nanorod growth inside a pore channel, such evolution selection growth is likely to lead to the formation of a single crystal nanorod or a bundle of single-crystal nanorods per pore channel (Fig. 5(a)). It is well known that [010] or *b*-axis is the direction of fastest growth for a V_2O_5 crystal,[28,29] which

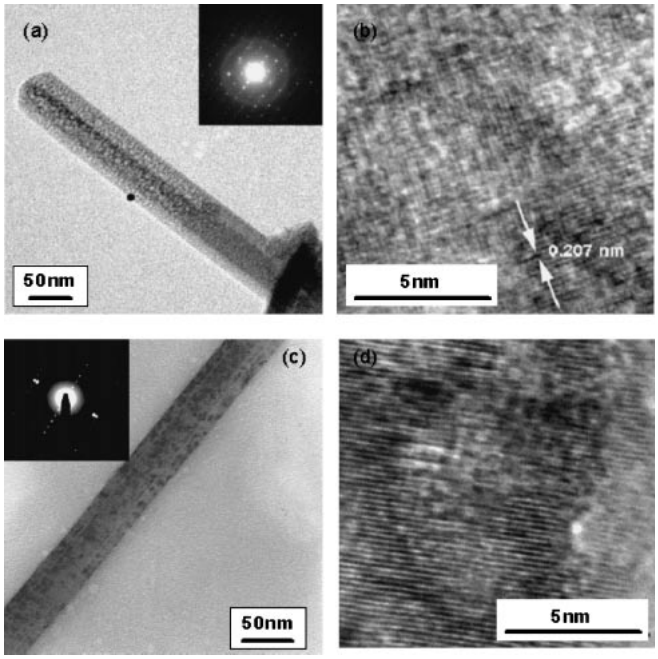

Fig. 4. TEM images of V_2O_5 nanorod grown into the membrane with 200-nm-diameter pores and its electron diffraction patterns.

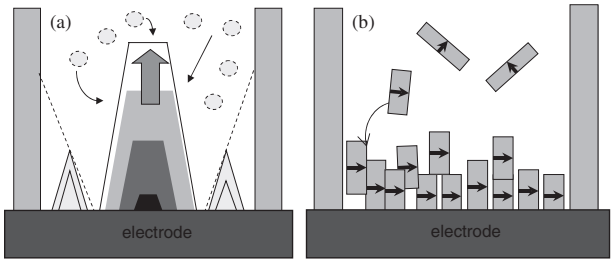

Fig. 5. Schematic illustrations of growth mechanisms of single crystalline nanorods: (a) evolution selection growth, (b) homoepitaxial aggregation.

would explain why single-crystal vanadia nanorods or a bundle of single crystal nanorods grow along the b-axis.

In the case of nanorods made from sol by electrophoretic deposition, the formation of single-crystal nanorods is explained by the homoepitaxial aggregation of crystalline nanoparticles. Thermodynamically it is favorable for the crystalline nanoparticles to aggregate epitaxially; such a growth behavior and mechanism have been thoroughly reported in the literature.[30,31] In this growth mechanism, an initial weak interaction between two nanoparticles allows rotation and migration relative to each other. Obviously homoepitaxial aggregation is a competitive process with close packing of nanoparticles, and thus a highly porous structure is expected to form through such homoepitaxial aggregation (illustrated in Fig. 5(b)). Vanadium oxide sol particles are known to form an ordered crystal-like structure easily,[32] so it is reasonable to expect that homoepitaxial aggregation of vanadia nanocrystals from sol results in the formation of single-crystal nanorods. Thus-formed single-crystal nanorods are likely to be highly porous and to undergo significant shrinkage when fired at high temperatures. In addition, the electric field and the internal surface of pore channels may all play a significant role in the orientation of nanorods, as suggested in the literature.[33,34]

It is also noted that the diameter of nanorods observed in TEM images (Fig. 4) is approximately 50 nm, which is much smaller than observed by SEM (Fig. 2), which was 150 nm to 200 nm. One possible explanation is that one large nanorod, as observed in SEM images, may consist of several smaller single-crystal nanorods, as seen in TEM images. Moreover, the sample preparation procedures for TEM analysis might promote such splitting. SEM micrographs of the nanorods were directly taken after removal of PC templates by pyrolysis at 485°C. For TEM, nanorods after pyrolysis were mixed with ethanol and subsequently subjected to 15 minutes of sonication to disperse nanorods. Sonication may result in not only branching and splitting of crystals but also delamination of V_2O_5 sheets into several smaller nanorods along the axis [010].

Figure 6 shows typical cyclic voltammograms of V_2O_5 nanorod arrays and sol-gel film measured using a scan rate of 1 mV/s. The cyclic voltammogram of nanorod arrays grown from shows one anodic oxidation peak at 0.0 V and a broad peak at −0.7 V, which is attributed to Li^+ extraction, and cathodic peaks at −0.3 and −1.1 V, which correspond to Li^+ intercalation. Artuso *et al.*[35] also reported similar IV curves that have a combination of one obvious anodic peak and two cathodic peaks. For sol-gel films, besides the anodic peak at 0.0 V, another anodic peak at −0.7 V is apparent. Furthermore, the cathodic peaks at −0.3 and −1.1 V are less distinct. The integrated area of IV curves for nanorod array and sol-gel film is similar, which implies that both nanorod arrays and films possess the same specific power at this scan rate. However, extraction and intercalation kinetics are different, as evidenced by the sharp peaks from the nanorods made from solution routes, as compared with far less distinctive peaks in the IV curve of sol-gel film. The behavior of the IV curve of sol-gel nanorods is intermediate between those of nanorods from solutions and sol-gel film, although the nanorods have single-crystalline structure.

For nanorod arrays, there is almost no Li^+ extraction other than in the vicinity of 0.0 V with a high discharge current (sharp and tall peak). Such a discharge behavior suggests that nanorod arrays may have no or very little current leakage and a high energy density output. Similarly the cathodic peaks in the IV curve of the nanorod array are considerably better defined. Such sharp peaks suggest faster intercalation reactions at given voltages. For the sol-gel film, both charge and discharge peaks are far less well defined, which suggests relatively slow extraction and intercalation processes.

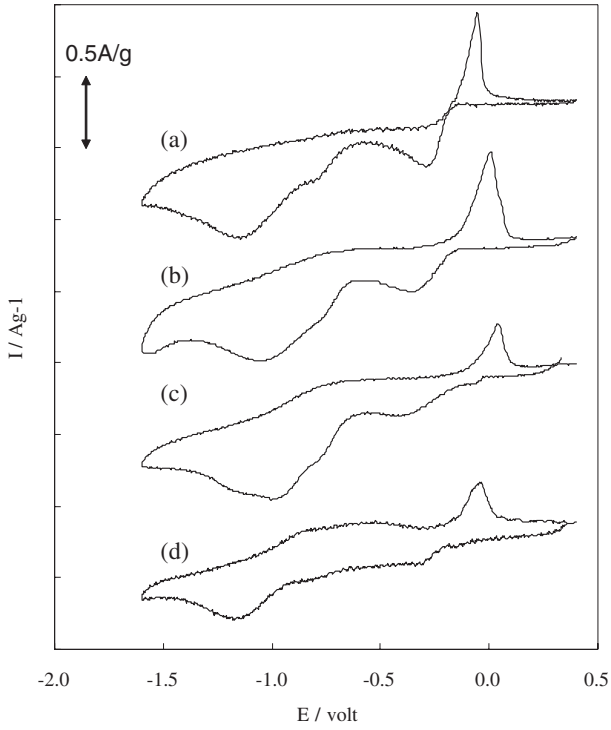

Fig. 6. Cyclic voltammograms of V_2O_5 nanorod arrays and sol-gel film measured using a scan rate of 1 mV/s (a) nanorods from $VOSO_4$, (b) nanorods from pH-change route, (c) nanorods from sol-gel electrophoresis, (d) sol-gel film.

Similarities between nanorod arrays fabricated by sol electrophoretic deposition and sol-gel-derived films suggest that the nanorod arrays formed by sol electrophoretic deposition are likely highly defective, with low angle boundaries, twins, stacking faults, and inclusion of pores.

Intercalation and extraction of Li^+ at 0.0, −0.7, −0.3, and −1.1 V involve different chemical reactions, resulting in the formation of different phases. $Li_xV_2O_5$ has three different phases at room temperature, which are α ($x < 0.1$), ε ($0.3 < x < 0.8$), and δ ($0.9 < x$) phases. IV curves suggest that the two cathodic peaks correspond to phase transitions from α to ε, and from ε to δ. The broad anodic peak at −0.7 V observed in sol-gel-derived film suggests that a concentration gradient of Li^+ in the V_2O_5 crystal exists during the extraction process, as reported by Cocciantelli.[36] The nanorod array electrode does not exhibit a peak at −0.7 V, but shows one large Li^+ extraction peak at 0.0 V, indicating that nanorod arrays possess minimal Li diffusion resistance.

Figure 7 shows the comparison between the current density and Li^+ insertion capacity of nanorod arrays and sol-gel films measured using chronopotentiograms. In gen-

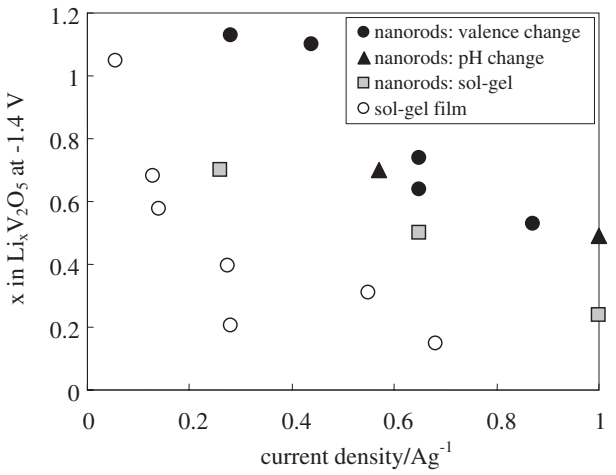

Fig. 7. Plot of discharge capacity versus current density for both V_2O_5 nanorod arrays and sol-gel-derived films.

eral, for a given Li^+ intercalation capacity, *e.g.*, $Li_{0.7}V_2O_5$, nanorod arrays fabricated via the solution route possess up to 5 times higher current density than do sol-gel films, and is larger than capacity of nanorods made by sol electrophoresis. Similarly for a given current density, such as 0.7 A/g, nanorod arrays can store up to 5 times higher Li than that in sol-gel films and about 1.5 times higher than in nanorods made from sol electrophoresis. The differences in electrochemical pseudocapacitor properties observed in vanadium pentoxide nanorod arrays and sol-gels films are attributed to the differences in microstructure and nanostructure. Vanadium pentoxide nanorods grown by electrochemical deposition are dense single crystals, with vanadia layers parallel to the nanorod axis. Such a structure is extremely favorable for Li^+ intercalation and extraction, since the surface oxidation and reduction reactions occur along the surface of nanorods and the solid state diffusion distance is very short, ~100 nm, which is half the diameter of nanorods. In addition, such a structure permits the most freedom to the dimensional change that accompanies intercalation and extraction reactions. Such a well-aligned structure would also enhance Li^+ diffusion through the solvent. The nanorod made by sol electrophoresis is also single crystalline and well aligned, but it has many defects inside the crystal. This may be the cause of the difference between these nanorod array electrodes. Sol-gel vanadia films are polycrystalline and consist of platelet vanadia grains with [001] perpendicular to the substrate surface. Therefore, the Li^+ intercalation and extraction processes would comprise Li^+ diffusion through grain boundaries, oxidation and reduction reactions at the surface of individual crystal grains, and diffusion inside individual grains. The difference in microstructure would have similar effects on the charge transport.

4. Conclusions

Single-crystal vanadium pentoxide (V_2O_5) nanorod arrays were grown by electrochemical deposition, surface condensation induced by a change of local pH as a result of H_2O electrolysis, and sol-gel electrophoretic deposition. Uniformly sized vanadium oxide nanorods with a length of about 10 μm and diameters ranging from 100 to 200 nm were grown over a large area, with nearly unidirectional alignment. Although the initial conditions and growth mechanisms are different, nanorods have single-crystalline structures orientated along the growth axis. The growth of single-crystal vanadium pentoxide nanorods via the solution route is attributed to the evolution selection growth mechanism, whereas nanorods grown by sol electrophoresis are built up by homoepitaxial agglomeration.

The current density and Li insertion capacity of nanorod array electrodes fabricated by electrochemical deposition have approximately up to 5 times higher applicable current density than do sol-gel-derived film and nanorods formed by sol electrophoresis. This suggests that the nanorod-electrode has faster intercalation reactions at a given voltage. The differences in electrochemical pseudocapacitor properties observed in vanadium pentoxide nanorods arrays and sol electrophoresis nanorods or films are attributed to the differences in the microstructure and nanostructure between them.

Acknowledgements

A portion of the research (TEM study) described in this paper was performed at the Environmental Molecular Sciences Laboratory, a national scientific user facility sponsored by the Department of Energy's Office of Biological and Environmental Research and located at Pacific Northwest National Laboratory. S. J. L. is grateful for the financial support from the NSF-IGERT fellowship from the Center for Nanotechnology at the University of Washington, and Y.W. for the Ford Motor Company Fellowship.

1) G. Z. Cao: *Nanostructures and Nanomaterials: Synthesis, Properties and Applications* (Imperial College Press, London, 2004).
2) *Encyclopedia of Nanoscience and Nanotechnology*, ed. H. S. Nalwa (American Scientific Publishers, Stevenson Ranch, CA, 2004).
3) *Nanowires and Nanobelts Materials, Properties and Devices*, ed. Z. L. Wang (Kluwer, New York, 2003).
4) Y. N. Xia and P. D. Yang: *Special Issue on Nanowires and Nanorods*, Adv. Mater. **15** (2003) No. 5.
5) D. N. Mcllroy, D. Zhang, Y. Kranov and M. G. Norton: Appl. Phys. Lett. **79** (2001) 1540.
6) Z. W. Pan, Z. R. Dai and Z. L. Wang: Science **291** (2001) 1947.
7) S. Iijima: Nature **354** (1991) 56.
8) C. R. Martin: Science **266** (1994) 1961.
9) T. M. Whitney, J. S. Jiang, P. C. Searson and C. L. Chien: Science **261** (1993) 1316.
10) A. Huczko: Appl. Phys. A **70** (2000) 365.
11) B. B. Lakshimi, C. J. Patrissi and C. R. Martin: Chem. Mater. **9** (1997) 1544.
12) Z. Miao, D. Xu, J. Ouyang, G. Guo, X. Zhao and Y. Tang: Nano Lett. **2** (2002) 717.
13) P. Sarkar and P. S. Nicholso: J. Am. Ceram. Soc. **79** (1996) 1987.
14) S. J. Limmer, S. Seraji, M. J. Forbess, Y. Wu, T. P. Chou, C. Nguyen and G. Z. Cao: Adv. Mater. **13** (2001) 1269.
15) S. J. Limmer, S. Seraji, M. J. Forbess, Y. Wu, T. P. Chou, C. Nguyen and G. Z. Cao: Adv. Funct. Mater. **12** (2002) 59.
16) P. Liu, S.-H. Lee, C. E. Tracy, J. A. Turner, J. R. Pitts and S. K. Deb: Solid State Ionics **165** (2003) 223.
17) G. Gu, M. Schmid, P. W. Chin, A. Minett, J. Fraysse, G.-T. Kim, S. Roth, M. Kozlov, E. Munoz and R. H. Baughman: Nat. Mater. **2** (2003) 316.
18) J. Livage: Chem. Mater. **3** (1991) 578.
19) T. Watanabe, Y. Ikeda, T. Ono, M. Hibino, M. Hosoda, K. Sakai and T. Kudo: Solid State Ionics **151** (2002) 313.
20) M. J. Parent, S. Passerini, B. B. Owens and W. H. Smyrl: Electrochimi. Acta **44** (1999) 2209.

21) T. Kudo, Y. Ikeda, T. Watanabe, M. Hibino, M. Miyayama, H. Abe and K. Kajita: Solid State Ionics **153** (2002) 833.
22) K. Takahashi, S. J. Limmer, Y. Wang and G. Z. Cao: J. Phys. Chem. B **108** (2004) 9795.
23) P. S. Devi and D. Ganguli: J. Non-Cryst. Solids **240** (1998) 50.
24) C. J. Fontenot, J. W. Wiench, M. Pruski and G. L. Schrader: J. Phys. Chem. B **104** (2000) 11622.
25) A. van der Drift: Philips Res. Rep. **22** (1968) 267.
26) G. Z. Cao, J. J. Schermer, W. J. P. van Enckevort, W. A. L. M. Elst and L. J. Giling: J. Appl. Phys. **79** (1996) 1357.
27) M. Ohring: *The Materials Science of Thin Films* (Academic Press, San Diego, CA, 2001).
28) D. Pan, Z. Shuyuan, Y. Chen and J. G. Hou: J. Mater. Res. **17** (2002) 1981.
29) V. Petkov, P. N. Trikalitis, E. S. Bozin, S. J. L. Billinge, T. Vogt and M. G. Kanatzidis: J. Am. Chem. Soc. **124** (2002) 10157.
30) R. L. Penn and J. F. Banfield: Geochim. Cosmochim. Acta **63** (1999) 1549.
31) C. M. Chun, A. Navrotsky and I. A. Aksay: *Proc. Microscopy and Microanalysis 1995*, p. 188.
32) J. Livage: Coord. Chem. Rev. **178–180** (1998) 999.
33) K. V. Saban, J. Thomas, P. A. Varughese and G. Varghese: Cryst. Res. Technol. **37** (2002) 1188.
34) D. Grier, E. Ben-Jacob, R. Clarke and L. M. Sander: Phys. Rev. Lett. **56** (1986) 1264.
35) F. Artuso, F. Bonino, F. Decker, A. Lourenco and E. Masetti: Electrochim. Acta **47** (2002) 2231.
36) J. M. Cocciantelli, M. Menetrier, C. Delmas, J. P. Doumerc, M. Pouchard, M. Broussely and J. Labat: Solid State Ionics **78** (1995) 143.